Power System Technology **Volume 46 · Number 2 · 2022**
ISSN: 1000-3673

Source-storage Configuration for User-side Integrated Energy System Based on Interval Linear Programming

Yang D., Shen Y., Jiang C., Xu Y., Ran Z., Nie F.1.
University of Bristol, United Kingdom
2. University of the West of England (UWE), Bristol, United Kingdom

ABSTRACT

An electrostatic ion thruster, modelled on Busek's BIT-3 [5], is simulated numerically using the open-source software "Starfish". It is assumed that the thruster is in vacuum conditions propelling a CubeSat in low Earth orbit. Iodine is chosen here as the propellant under test. The results from modelling this relatively recent new fuel are compared to those of the standard propellant of xenon. The plasma in the ion thruster and the associated electric fields are simulated using a particle-based kinetic code in which the hybrid approach of Particle in Cell and Direct Simulation Monte Carlo methods has been used. In modelling these flows, elastic and inelastic collisions can occur involving charge and momentum exchanges. Such collision models use a number of assumptions, e.g., concerning the collisional cross-section area, and in this paper, we present results where the physico-chemical modelling is improved reducing the level of assumptions used. Results are also presented concerning the numerical methods used for the iterative convergence scheme, stochastic sampling, and the importance of the constraints for the mesh size and timestep. It is found that the most appropriate timestep is one which enables both the CFL condition and the highest frequency to be captured. The mesh size affects the choice of the solver being used; the largest the cell sizes the greater the assumption of quasi-neutral flow and thus areas of non-neutrality (such as in the surrounding shealth may be treated inadequately. The subsequent effects on the plume and the thrust produced of using different approaches in modelling the electron temperature distribution are also evaluated to produce a more rigorous modelling methodology.

1. INTRODUCTION

Ion thrusters or ion drives are an established successful method of in-space electric propulsion. They are categorised as either electrostatic or electromagnetic. In this paper, the results of numerically simulating an electrostatic ion thruster propelling a CubeSat in a low Earth orbit using the open source software "Starfish" are presented. It is assumed that the thruster is in vacuum conditions propelling a CubeSat in low Earth orbit. The plasma in the ion thruster and the associated electric fields are simulated using a particle-based kinetic code in which a hybrid approach of Particle in Cell and Direct Simulation Monte Carlo methods has been used. Elastic, inelastic, charge and momentum exchange collisions are taken into account

throughout the simulations. Some assumptions in the previous mentioned collision models such as the collision cross-section are reviewed in this paper as well as presenting the results where the physico-chemical modelling is improved reducing the level of assumptions used. This paper is organised as follows: section 2 introduces ion thrusters; section 3 provides the definitions and theories used in modelling electrostatic ion thrusters. Since these ion drives rely on propellants to provide the mass to convert to the exhaust ion jet, the popular xenon is compared to the newer fuel iodine. The methodology and setup for the simulations is presented in section 5 to 7. Results are shown in sections 8 (comparison of xenon and iodine) and 9 (development of modelling using Iodine fuel). Conclusions on the modelling are discussed in section 10.

The subsequent effects on the ion plume emitted from the ion drive and the thrust produced of using different approaches in modelling the electron temperature distribution are also evaluated to produce a more rigorous modelling methodology.

2. ION THRUSTERS

2.1. Mission scenario

An ion thruster is an electric propulsive device utilised for space missions. Due to the ion thrusters' small compact size, high efficiency and high specific impulse, they are used for a wide variety of missions and utilised in different types of satellites. They are now more commonly seen in nanosatellites (CubeSats) for orbit manoeuvrability/altitude correction and to lower a mission's operational cost due to it being able to extend the operational life of the satellite.

2.2. Thrust Geometry and main components

The three main components which can be said to compose an ion thruster are the plasma generator, accelerator grids and the neutralizer cathode [7].

The propellant is ionized to form plasma, which (Figure 1) is produced by the discharge cathode and anode. The plasma is generated by firing electrons at the propellant which results in positive ions and electrons. The ions from this region flow into the accelerator grid which accelerates them into a beam. Due to the ions leaving the thruster being positively charged, the neutralizer cathode is used to fire electrons into the beam at the same rate as ions leaving in order to keep the overall charge neutral to avoid charge imbalance with the spacecraft. The plasma generator is usually also kept in an enclosure called the plasma screen, in order for the overall positive charge not to be affected by electrons in the plume.

2.3. Thrust Generation

In order to produce thrust, a change in momentum must occur. The force produced by the thruster is generated by the mass flow rate of the ions times their change in speed from when they leave the thruster. Ion thruster inefficiencies come from the ionization of the propellant used and other electrical losses.

Higher thrust can be achieved in ion thrusters by decreasing a particle's velocity or increasing the mass flow rate for the given thruster set-up. This is due to the relationship of thrust exerted being proportional to the velocity squared. Thus, for a given mass flow rate, thrust can be increased by increasing the particle speed but at the cost of increasing the power consumption of the thruster. Power consumption is proportional to the particle velocity cubed.

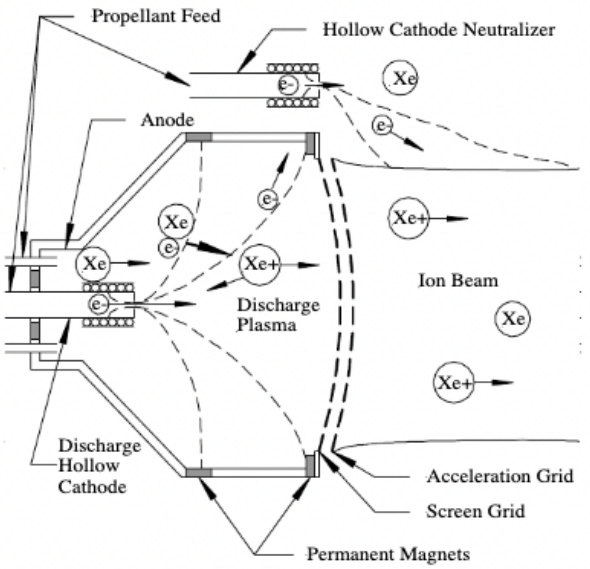

Figure 1. Ion thruster geometry [12]

3. PLASMA SIMULATION

In this section are presented definitions of the concepts used in the modelling.

3.1. Particle in Cell and other algorithms utilized

Three models are utilized in this study:

- The Electrostatic Particle in Cell (ES-PIC) method is used to model plasma.
- The Monte Carlo Collision (MCC) model is utilized to model particle collisions alongside the Direct Simulation Monte Carlo (DSMC) method. MCC considers the acceleration exerted only by electromagnetic forces, whereas DSMC considers a neutral gas and only models collisions. These two methods are also examples of stochastic sampling where velocity "bins" (i.e., subdivisions of the velocity distribution function) containing a low number of particles (including zero) are assigned a random number of velocity samples with a given probability representing the distribution function used [4].

3.2 Assumptions when modelling plasma

Plasma is a gas comprised of neutrons, charged positive ions, and electrons. Other multiphase flows involving gas components are not taken into account in this paper. The objective of the simulations performed is to solve the governing physical equations subject to initial conditions so as predict the evolution of the particles' positions and velocities once ejected from the thruster.

A kinetic approach is used throughout which, in comparison to fluid approaches, does not make any assumptions on the shape of the velocity distribution function (VDF) and instead allows it to develop consistently [4]. A constant particle specific weight is assumed for all simulations performed. A constant particle specific weight is assumed for all simulations performed.

3.3. Boltzmann Equation

The Boltzmann equation (Equation 1) describes the development in space and time of the particle density of a plasma, where f is the particle distribution function. The three-dimensional function, f, depends on position (x, y, z), velocity $v = (u, v, w)$ and time, t, i.e., $f = f(x, y, z, u, v, w, t)$. ∇ is the vector differential operator, F is the force vector and m is the (identical) mass of each particle.

$$\frac{\delta f}{\delta t} + \nabla \cdot f + \frac{F}{m} \nabla_v \cdot f = \left(\frac{\delta f}{\delta t}\right)_{col} \tag{1}$$

3.4. Lorentz Force

The equation of motion for a charged particle with a specified velocity, v, in a magnetic field, B, is given by the Lorentz force equation (Equation 2).

$$F = q(E + v \times B) \tag{2}$$

where q is the particle charge and E is the electric field.

3.5. Maxwell's Equations

Electric and magnetic fields that are present in electric propulsion obey Maxwell's equations which are the fundamental equations of electromagnetics. These equations consider a vacuum that contains charge densities and current densities (Equations 3-6).

$$\nabla \cdot E = \frac{\rho}{\epsilon_0} \tag{3}$$

$$\nabla \times E = -\frac{\delta B}{\delta t} \tag{4}$$

$$\nabla \cdot B = 0 \tag{5}$$

$$\nabla \times B = \mu_0 \left(J + \epsilon_0 \frac{\delta E}{\delta t}\right) \tag{6}$$

where ρ is the charge density, ϵ_0 is permittivity of free space, μ_0 is permeability of free space and J is the electric current density.

The charge density, ρ, is given by Equation (7).

$$\rho = \sum_S q_s n_s = e(Z n_i - n_e) \tag{7}$$

where S is the surface being integrated, e is the elementary charge, Z is the charge state, n is number density and subscripts i and e denotes ionic and electron respectively.

Likewise, the electric current density, J is given by Equation (8).

$$J = \sum_S q_s n_s v_s = e(Z n_i v_i - n_e v_e) \tag{8}$$

For a static magnetic field ($dB/dt = 0$), the electric field (E) is represented as the electric potential gradient in Equation (9). This assumes that the current density is low enough for the self-induced magnetic field to be considered negligible.

$$E = -\nabla v \tag{9}$$

The negative sign denotes the convention for the electric field to be in the same direction as the ion motion. Substituting equation 9 into Gauss' equation produces Poisson's equation for the electric potential, ϕ (Equation 10).

$$\nabla^2 \phi = -\frac{\rho}{\epsilon_0} \tag{10}$$

The Poisson equation is the underlying equation for the electrostatic particle-in-cell method.

3.6. Plasma Sheath

When assuming plasma quasi-neutrality, the ratio of electron to ion current density is given by Equation (11).

$$\frac{J_e}{J_i} = \frac{v_e}{v_i} = \sqrt{\frac{m_i T_e}{m_e T_i}} \tag{11}$$

Due to the ions having a bigger mass than the electrons, the electron flux is significantly larger than the ion flux, making it impossible to hold a quasi-neutral state. Considering how electrons have a much higher temperature than ions, the ratio of electron flux to ion flux is further increased. The difference in current densities causes the generation of electric fields that slow down the electrons and ensures that the quasi-neutral condition is maintained. When utilizing the quasi-neutral assumption, the electrons are modelled as a Boltzmann fluid.

Near the walls of the ion thruster, a non-neutral region develops, known as a sheath. In this region, the ion density is higher than the electron density, resulting in the formation of a bulk of plasma with an overall positive potential with respect to the wall. However, negative charged sheaths are also possible [7].

3.7. Debye Length

The radius of the smallest sphere which contains the same number of positive and negative charges is given by the Debye length (Equation 12). A sheath normally has a thickness of several Debye lengths.

$$\lambda_D = \sqrt{\frac{\epsilon_0 k_B T_e}{n_0 e^2}} \tag{12}$$

The thickness of a Debye sheath is minimal compared to that of the mean collision-free path in the plasma. External to the sheath, the plasma remains quasi-neutral as the electrons and ions cannot detect the sheath. This effect is known as the Debye shielding, which is the capability of the plasma screening out potential disturbances.

3.8. Knudsen number

The Knudsen number (Equation 13) is a vital factor in the modelling; it relates the mean free path to a characteristic length.

$$K_n = \frac{\lambda}{L} \tag{13}$$

When $K_n < 1$, it is assumed that each molecule undergoes many collisions as it travels between walls. A Maxwellian velocity distribution function is applied. When $K_n > 1$ no collisions occur, and a free molecular flow exists (molecules are more likely to collide with the wall). When K_n is approximately 1, the distance between the collisions is similar to that of the characteristic length, so collisions occur but infrequently and the Maxwellian distribution function cannot be used with certainty [4].

4. ION THRUSTER PROPELLANTS

4.1. Xenon

Xenon is currently the most common propellant used in ion thrusters. It is a noble gas, which is easily ionized. Its high atomic mass generates desirable levels of thrust when the ions are accelerated [6]. Many studies on modelling xenon ion thrusters exist now as well as a significant number of physical testing reports which can be used to validate numerical simulations. Having more data available (such as propellant cross sections, collisional cross sections and mathematical models which account for the variation in collision cross section in relation to speed) increase the accuracy of the results by reducing the number of assumptions needed.

A significant drawback of using xenon as a propellant is its expense. This leads into researching into other propellants with similar element characteristics that could lead to comparable performance but at a lower cost, such as iodine, which is the propellant used throughout this study.

4.2. Comparison of Iodine and Xenon Properties

Table 1 compares iodine and xenon properties. When storing the propellant in an ion thruster, iodine has a clear advantage due to its solid density (iodine has 4.933 g/cm^3 to that of 1.6 g/cm^3 of xenon). Iodine is also significantly cheaper than xenon. Iodine has a very low storage vapour in comparison to that of xenon. This allows for the reservoir tank to have thinner walls and to be made out of lighter materials. However, xenon is a non-toxic inert gas, whereas iodine in large amounts is toxic and reactive, thus protective equipment is needed for handling iodine. Consideration also needs to be made ensuring the choice for the materials the thrusters are made from so that no reactions with iodine occur. These, therefore, impact on the cost of manufacturing and production [11].

Table 1. Comparison between element characteristics between iodine and xenon [11]

	I	**Xe**
Atomic mass (g/mol)	126.9	131.3
First ionization potential (eV)	10.5	12.1
Peak cross section (1e-16 cm^2)	6.0	4.8
Solid density (g/cm^3)	4.933	1.6
Storage vapour pressure (Torr at $-75°C$)	1.2×10^{-6}	4.0964×10^{3}

5. AVAILABLE SOLVERS

5.1. Poisson solver

There are two approaches to solving the Poisson equation. In linear mode, the electron density is computed from the electrons. In nonlinear mode, Equation (14) is solved alongside with Equation (15) to obtain the electron density.

$$\varepsilon_0 \nabla^2 \phi = -e(n_i - n_e) \tag{14}$$

$$n_e = n_0 e^{\frac{\phi - \phi_0}{kT_{e0}}} \tag{15}$$

5.2. Boltzmann solver

The approach to solving the Boltzmann equation is to use a quasi-neutral solver (Equation 16). The assumption is that a state of quasi-neutrality is achieved in plasma thruster simulations due to the high densities in the core [4].

$$\phi = \phi_0 + kT_{e0} ln\left(\frac{n}{n_0}\right) \tag{16}$$

Electrons are assumed to be thermalized in the case of unmagnetized plasma and it is assumed that the number densities of the ions and electrons are equal.

5.3. Hybrid solver

In this solver the Poisson and Quasi-Neutral solvers are combined. The plume interactions are solved with the quasi-neutral solver as it provides significant flow detail quickly whereas the more expensive Poisson solved is used to capture the plasma sheath generated around the satellite.

This solver works by first analysing the Debye length (section 3.7) at each grid cell (size dx, dy) prior to iterations. If the Debye length is smaller than the cell spacing, then that node will be flagged as quasi-neutral and the Boltzmann solver would be used. Else the non-linear Poisson solver is used [1].

6. SIMULATION PARAMETERS

6.1. Domain and Boundary Conditions

The chosen domain has a size 20 times the length of the thruster's exit grid in the x-axis, and in the y axis,10 times the length of the thruster exit grid. This results in a domain with length 0.25m by 0.125m. At ambient domain boundaries where plasma neutrality is assumed (i.e., left, top and right of the thruster), the zero Neumann condition is applied. The exit plane of the thruster has Dirichlet conditions. The bottom surface is set to symmetry (Figure 2). Note that the flow is from left to right in all diagrams shown.

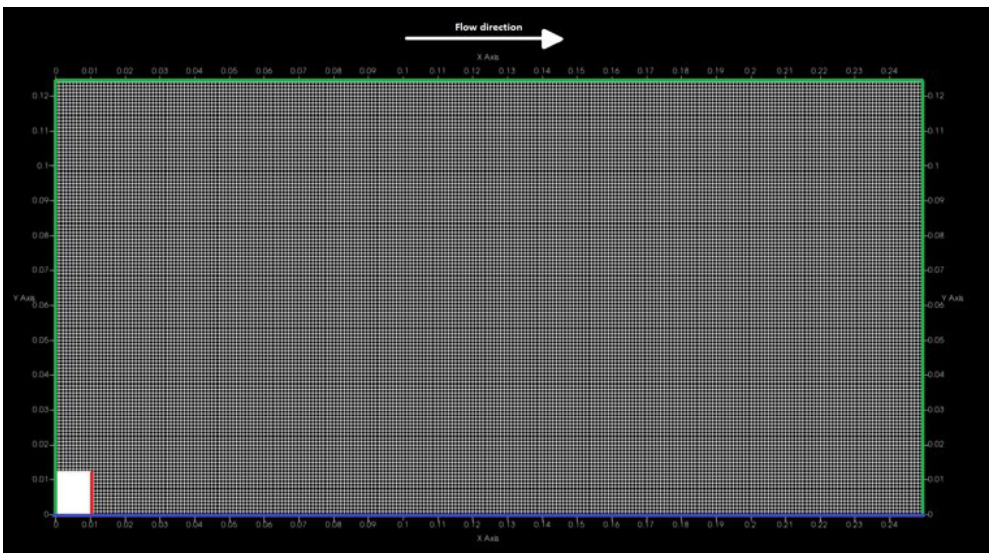

Figure 1. Domain set-up including mesh size illustration. A blue boundary denotes symmetry, green boundaries have Neumann boundary conditions, whereas the red boundary for the flow existing the thruster outlet has a Dirichlet condition applied. The mesh is fixed (not dynamic).

6.2. Time-step

The time-step value has a major impact on the thruster plume results. This is mainly because it must be small enough to ensure that particles cannot travel more than one cell length per iteration, i.e., CFL condition (Equation 17), as well as resolving the highest frequency (Equation 18). When the time-step is not small enough, the particles will not detect the electric field as continuous.

$$\Delta t < \frac{\Delta x}{v_{max}} \tag{17}$$

$$\omega_p = \sqrt{\frac{n_e e^2}{\varepsilon_0 m}} \tag{18}$$

To ensure the CFL condition when determining the time-step, the lowest value from Equations (17) and (18) is used [4]. The effect on the results of using different timesteps is demonstrated in Figures 3 & 4. As the timestep is increased, the spread of the plume increases, as it can be seen in the top half of Figure 3 some oscillations occur, this is due to not meeting the requirement of the CFL or the plasma frequency. On the other hand, if the time-step is too low, the simulation will take significantly more time to achieve very similar results for the total simulated time.

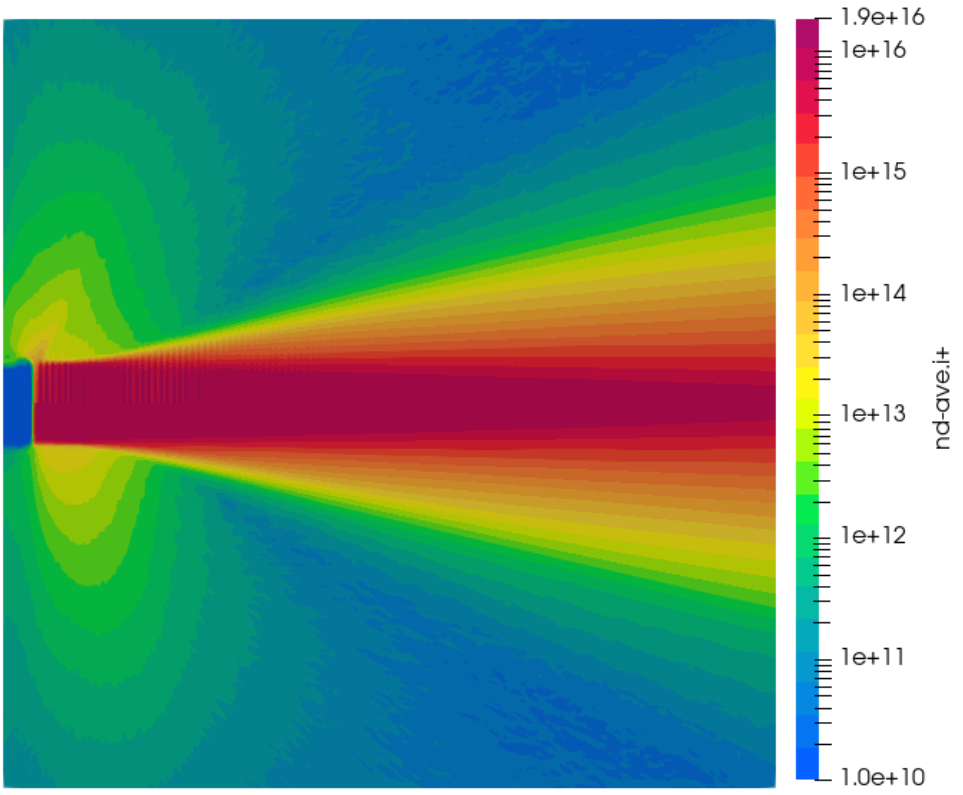

Figure 3. Comparison of two iodine simulations for a time step of 1×10^{-8} (bottom) and 5×10^{-8} (top) The Ionized iodine number density is shown.

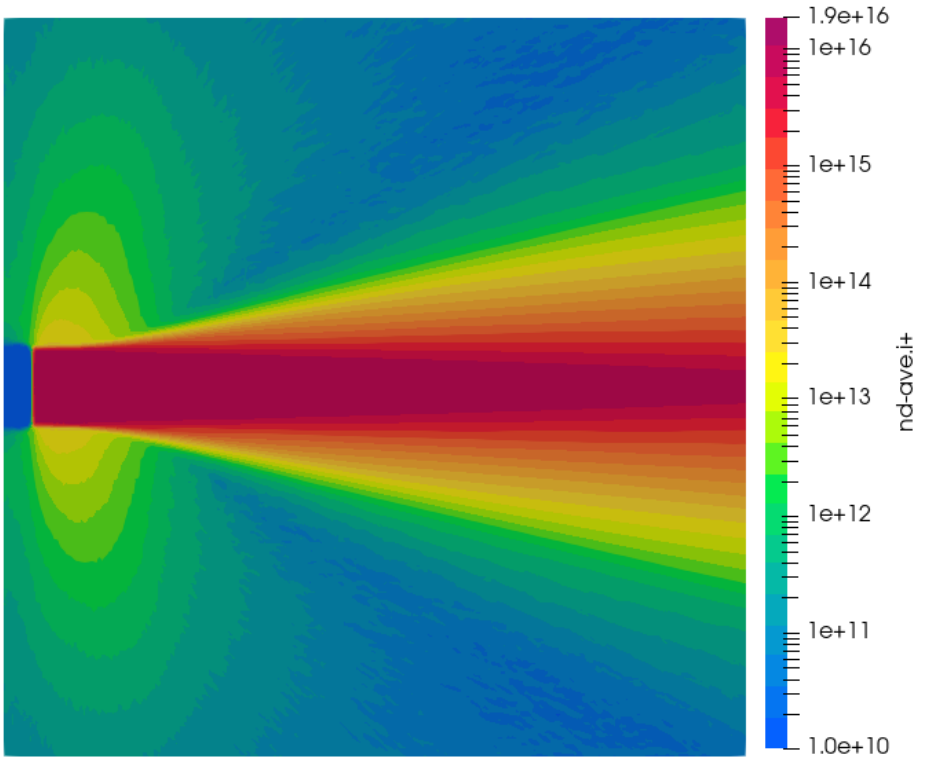

Figure 4. Comparison of two iodine simulations for a time step of 1×10^{-8} (bottom) and 5×10^{-9} (top) The Ionised iodine number density is shown.

6.3. Variable particle update

An additional algorithm has been implemented into Starfish as part of this study. Since the (thermalised) neutral particles travel at relatively slow speeds compared to the ionized particles, the simulation depends on the neutral particle transit time across the domain. The algorithm evaluates after how many time-steps a kinetic particle's velocity component should be updated; this produces a reduction in the simulation iterations without affecting the accuracy of the flow field, thus increasing the efficiency of the run.

6.4. Molecular specific weight

During the plasma presence, it is necessary to store a particle's position, velocity and specific (or macroparticle) weight (Equation 19). Normally it can be assumed that all particles share the same weight, and this assumption is kept throughout this study for generality. The specific weight is directly linked to the number density of the particles being simulated (Equation 20) [4].

$$\omega_{mp} = \frac{N_{real}}{N_{sim}} \tag{19}$$

$$N_{real} = nV \tag{20}$$

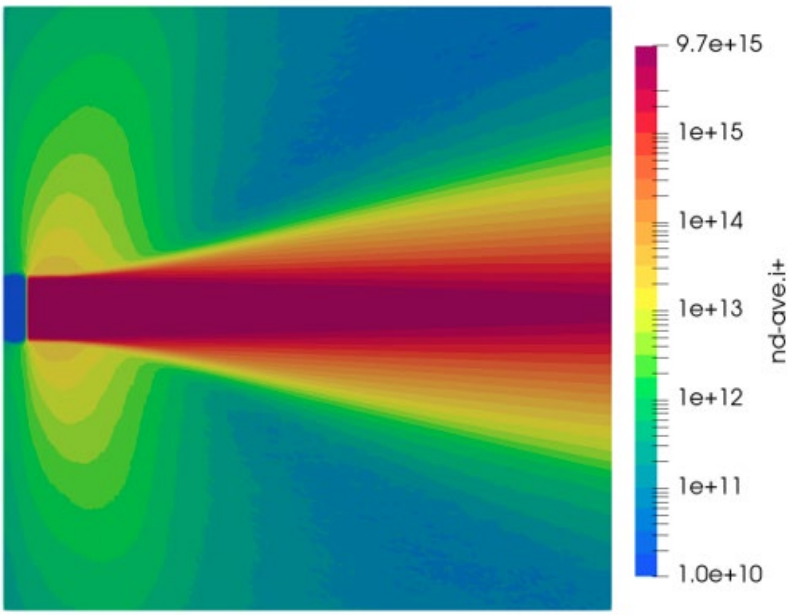

Figure 5. Comparison of two Iodine simulations with a molecular specific weight of 1×10^6 (bottom) and 5×10^5 (top). The Ionised iodine number density is shown.

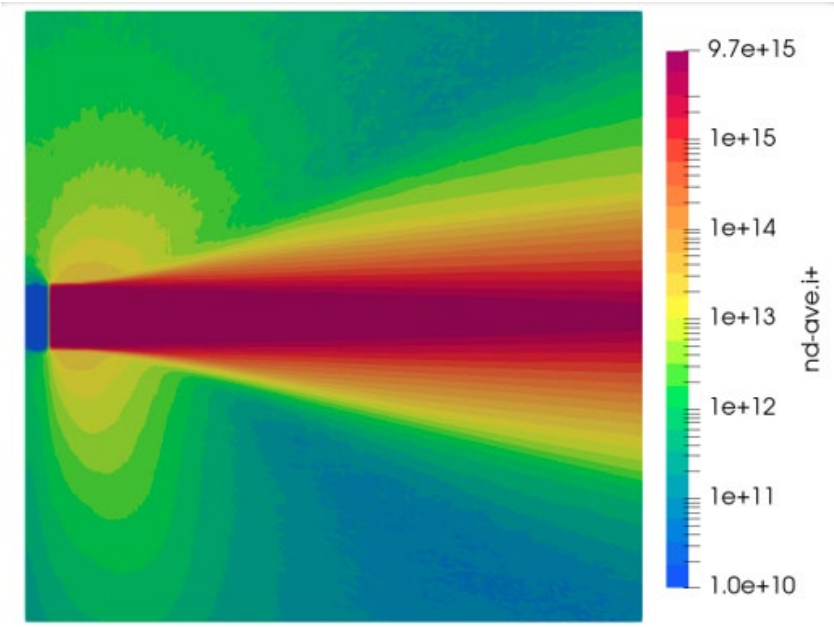

Figure 6. Comparison of two Iodine simulations with a molecular specific weight of 1×10^6 (bottom) and 1×10^7 (top). The Ionised iodine number density is shown.

Figure 5 shows how utilizing a molecular specific weight between 1×10^6 and 5×10^5 will result in very similar results. However, the 5×10^5 simulation required significantly longer computational time and achieves very similar plume results. Figure 6 shows that this is not the case for the specific weight of 1×10^7. The numerical noise increases due to the random particle loading as well as the reduction in particles per cell and this reduces the number of collisions possible. Figures 5 & 6 therefore show that the best suited configuration for this specific case is that of 1×10^6 due to the high resolution of data captured in a reasonable computational time. Choosing a lower molecular specific weight results in increases the particle density and the number of possible collisions, but at increased computational cost.

7. COLLISION MODELS

There are two types of collision exchange and a variety of collision models.

7.1. Momentum Exchange Collision

During a momentum exchange collision, a high velocity particle transfers energy to a slower particle causing thermalization of the velocity distribution function. The Direct Simulation Monte Carlo (DSMC) is used here for modelling Momentum Exchange Collisions [2].

7.2. Charge Exchange Collision

A charge exchange collision consists of an electron with the required transfer energy moving from the particle it currently belongs to a new particle nearby. This is a common type of collision when modelling ion thrusters due to their working mechanism making the ionised propellant leave the thruster with very high velocities whereas the neutral molecules have (by comparison) very low velocities. This results in backflow of some slow-moving ions due to the electric field force exerted on them. Charge exchange collisions are simulated by using the Monte Carlo Collision model [3]. Note that no momentum exchange occurs here.

7.3. Hard Sphere Model

Of the available collision models, some, such as the “soft sphere” model are computationally intensive. Less expensive is the “variable hard sphere” model. In this study the “hard sphere” model (Equation 21), which less expensive than the variable hard sphere model, is used as it is suitable for modelling the collisions between neutral iodine particles due to the assumption that most collisions have a high angle post-collision. This results in isotropic particle scattering.

$$\sigma_{HS} = \pi d_{12}^2 \tag{21}$$

where d is the collision diameter and σ is the collisional cross-section. Note the diameter is the sum of the radii of each particle.

7.4. MCC and DSMC Comparison for different propellants

The types of possible collisions vary between xenon and iodine with different probabilities of collision in the plume (see Tables 2 & 3). For xenon [1] it was shown how for a collision

between a Xe and Xe+ particle there is a 50% chance of it being a CEX or MEX collision. However, this information is not available for iodine, and therefore the assumption is made that the interactions between I2-I+ and I2-I2+ mainly consists of CEX collisions.

Table 2. Definition of particle collision algorithms for xenon simulations

	Xe	**Xe+**
Xe	MEX	CEX & MEX
Xe+	CEX & MEX	-

Table 2. Definition of particle collision algorithms for iodine simulations

	I2	**I+**	**I2+**
I2	MEX	CEX	CEX
I+	CEX	-	-
I2+	CEX	-	-

The difference in choice of collision model is shown in Figure 7 where the top half shows the results from using charge exchange collisions only, whereas the bottom half of the diagram shows the effects of modelling change and momentum exchange collisions (the quasi-neutral model). Note how the quasi-neutral model predicts less spread in the plume and less numerical noise in the solution.

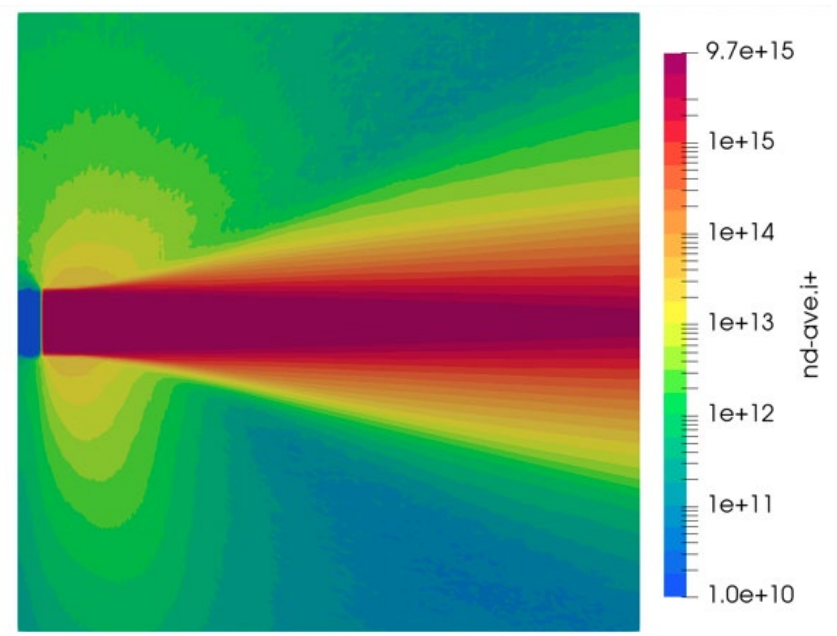

Figure 7. MCC (top) comparison against (quasi-neutral) hybrid MCC-DSMC (bottom). The Ionized iodine number density is shown.

8. MATHEMATICAL COLLISION MODEL COMPARISON STUDY

There are a number of approaches available for simulating a charge exchange collision (CEX), each model adopting slightly different assumptions. The CEX collision model chosen here for the interactions between the iodine particles is the model of Pullin et al (2002) (Equation 23) [9]. The results are compared to those from using the well-known Rapp & Francis (1962) model (Equation 22) [10]. The comparison case (same domain and setup apart from the CEX model) is for a xenon ion thruster. The results are illustrated in Figure 8. In order to simulate the collision cross section between the ionic iodine dimers and the neutral iodine particles, equation 25 is used (i.e., hard sphere model, section 7.3).

$$\sigma_{cex} = (k_1 ln(g) + k_2)^2 \cdot 10^{-20} \tag{22}$$

$$\sigma_{cex}(I^+, I_2) = A - B \cdot log(E) \tag{23}$$

$$\sigma_{cex}(I_2^+, I_2) = c_1 log^3(E) + c_2 log^2(E) + c_3 log(E) + c_4 \tag{24}$$

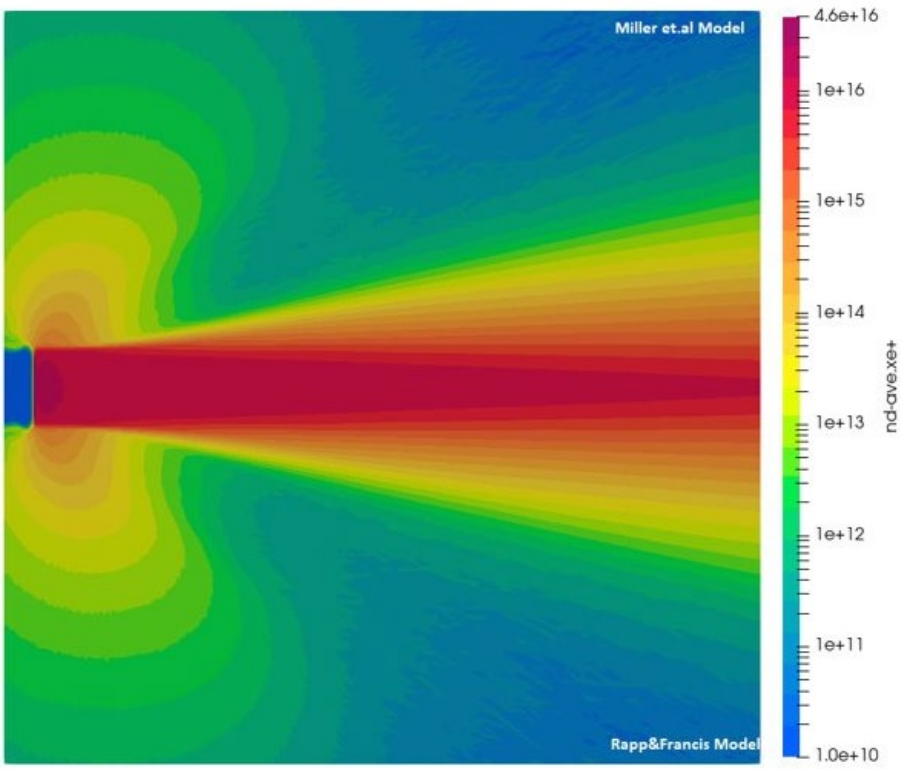

Figure 8. Comparison between Rapp & Francis [10] and Miller et.al [9] model results illustrating the plasma density for ionized xenon

As can be observed from the simulation results, both models agree due to the similarity in the plume contours, as well as the indicated density in the thruster plume. This implies that Equation 23 is suitable for simulating iodine collisions as both resulted in similar results in very similar computational time.

9. MODELLING IODINE

9.1. Introducing ionic iodine dimers

For an iodine powered ion thruster, the reactions can generate two types of ion: I+ and I2+, A comparison is presented here of results for a case where ionic iodine dimers I2+ (consisting of 20% of the plume [13]) are modelled against a case without ionic iodine dimers. This is illustrated in Figures 9 and 10.

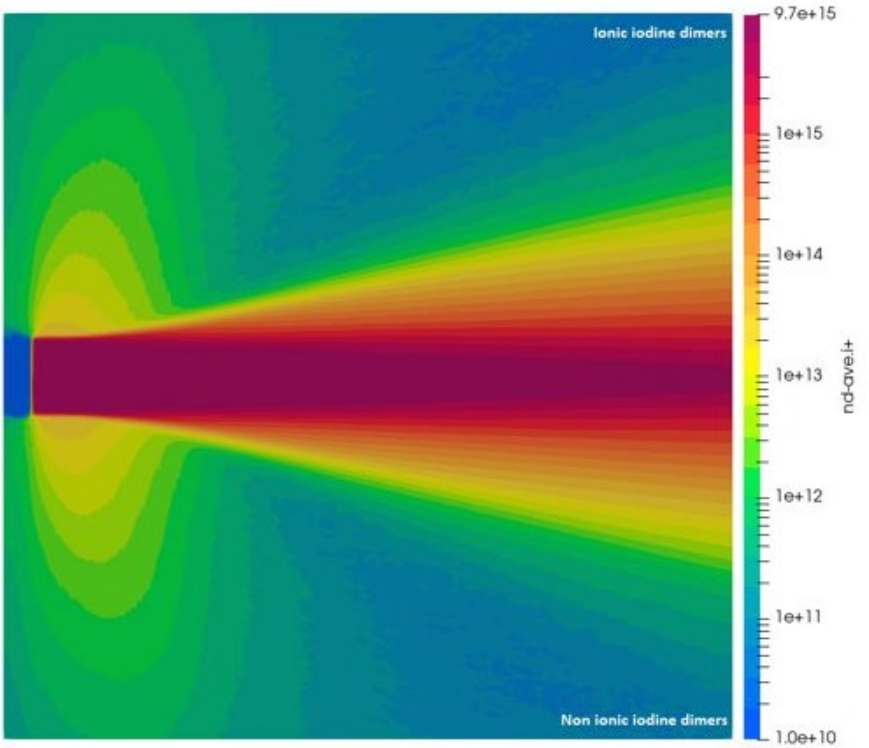

Figure 9. Comparison between a simulation with (top) ionized ionic iodine dimers I2+ and without (bottom). The distribution of Ionized iodine number density for I+ is shown.

The results obtained for the plasma density of I+ (Figure 9) are very similar, however there are major differences when viewing the effect of the introduction of I2+ (Figure 10). The differences in the plume shape and contour distribution are due to the difference in molecular mass between I+ and I2+. However, the spread due to the CEX collisions is still consistent. It is noted that in order to simulate I2+, a significant increase in computational time is required, to allow for the additional collisions in the domain.

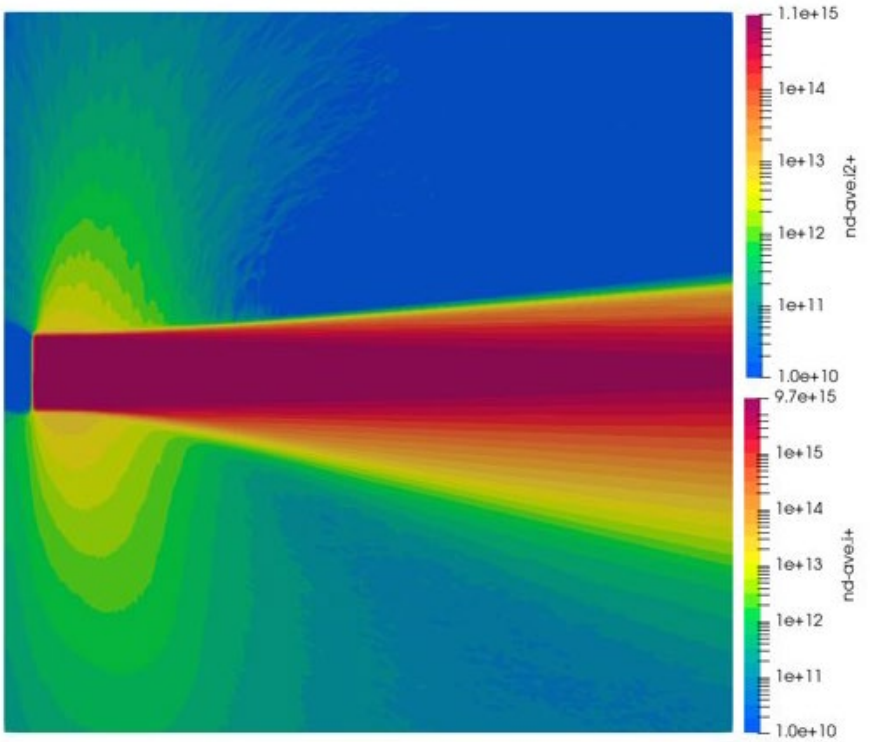

Figure 10. Comparison between a simulation with (top) ionized ionic iodine dimers I2+ and without (bottom). The distribution of Ionized iodine number density for I2+ is shown.

9.2. Electron temperature study

The electron temperature is known to affect the ion thruster plume results but there is a lack of current data available. Here an electron temperature study is performed where the temperature is varied from 1eV to 10eV in increments of 3eV. The results are illustrated in Figures 11-13.

The obtained results illustrate how the plasma density in the contour of the core of the plume is higher for an increase in electron temperature (Figure 11). Furthermore, the increase in electron temperature causes an overall decrease in plasma potential throughout the domain except for the core section of the plume (Figure 12). The charge density also varies with the electron temperature, as the electron temperature increases the charge density decreases in the charge exchange collision location (near the thruster exit) as it can be seen by comparing the electron temperature of 1eV to 10eV in Figure 13. However, the charge density has an overall increase around the contour of the plume.

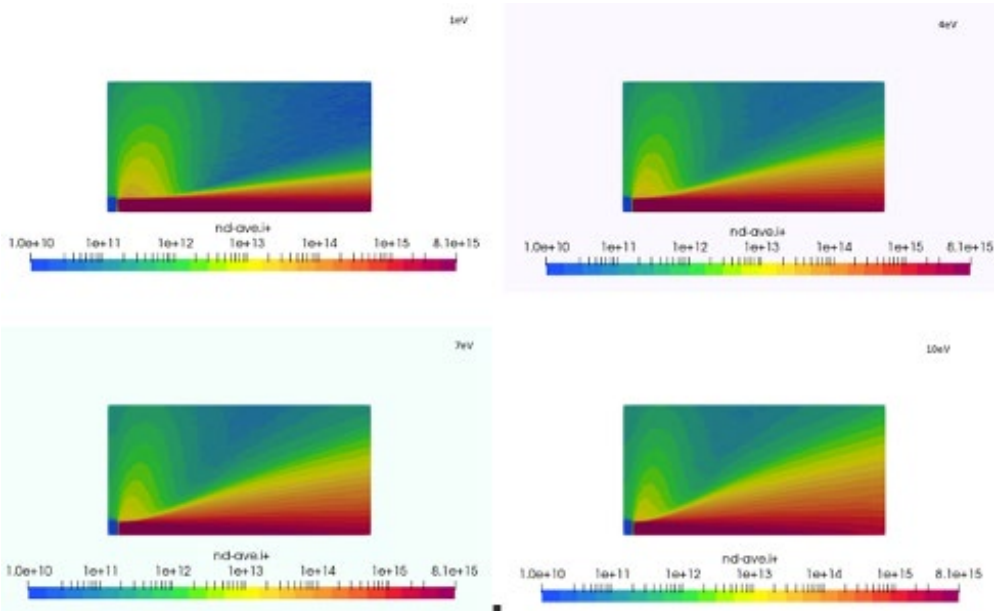

Figure 11. Electron temperature study from 1eV to 10eV illustrating ion density

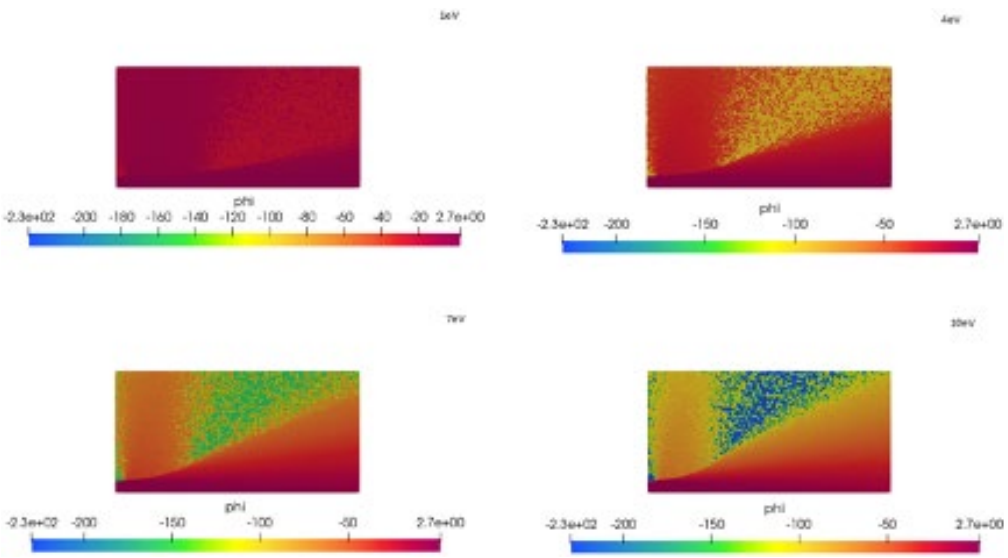

Figure 12. Electron temperature study from 1eV to 10eV illustrating plasma potential

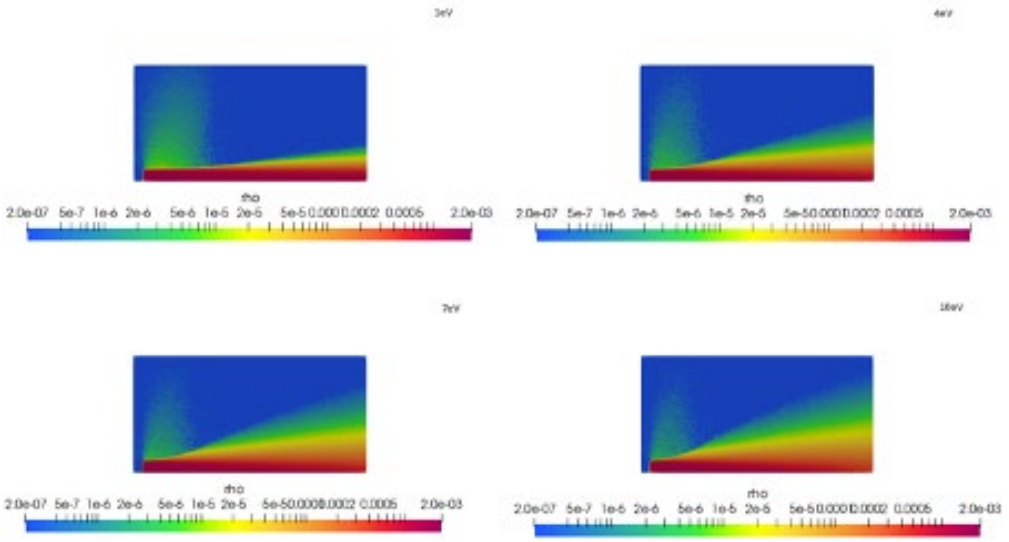

Figure 13. Electron temperature study from 1eV to 10eV illustrating charge density

10. CONCLUSION

This study has presented results for both conventional xenon and the alternative propellant, iodine. A series of numerical experiments were undertaken to study the effects on flow field accuracy and computational cost of varying timestep, collision models, and solvers. If the timestep is too high, some collisions are unaccounted for and thus missed in the simulation. Therefore, the minimum requirement is that of meeting the CFL condition which is directly linked to the fastest moving particle in the computational domain. The different solvers reviewed in this paper demonstrate the main differences in the plume detail capturing, and its relation to computational time. The study demonstrates the usefulness of having more than one solver option to utilise depending on which part of the plume or expansion is being studied. Another aspect covered in this paper is the effect of different collision models on simulating the plume, resulting in the best combination being that of a hybrid DSMC-MCC scheme.

A combination of the different experiments shows how to optimize computational time and power in order to capture different stages of the plume. However, it must also be noted that increasing the physical modelling of the system would result in better accuracy, less approximations and assumptions, but would increase the computational demands on the required processing time.

REFERENCES

[1] Andrews S, Berthoud L. Effect of Ion Thruster Plume-Thermosphere Interaction on Satellite Drag in Very Low Earth Orbit. 70th International Astronautical Congress (IAC). 2019.

[2] Bird G. Molecular gas dynamics and the direct simulation of gas flows. Oxford University Press; 1994.

[3] Birdsall C. Particle-in-cell charged-particle simulations, plus Monte Carlo collisions with neutral atoms, PIC-MCC. IEEE Transactions on Plasma Science. 1991;19(2):65-85.

[4] Brieda L. Plasma Simulations by Example. [S.l.]: Routledge; 2021.

[5] BIT-3 RF Ion Thruster — Busek [Internet]. Busek. 2022 [cited 5 February 2022]. Available from: https://www.busek.com/bit3

[6] Fazio N, Gabriel S, O. Golosnoy I. Alternative propellants for gridded ion engines. Space Propulsion. 2018.

[7] Goebel D, Katz I. Fundamentals of electric propulsion. Hoboken, N.J.: Wiley; 2008.

[8] Maria C. Modeling an Iodine Hall Thruster Plume in the Iodine Satellite (ISAT). (NASA Glenn Research Center Cleveland, OH United States); 2016.

[9] Miller J, Pullins S, Levandier D, Chiu Y, Dressler R. Xenon charge exchange cross sections for electrostatic thruster models. Journal of Applied Physics. 2002;91(3):984-991.

[10] Rapp D, Francis W. Charge Exchange between Gaseous Ions and Atoms. The Journal of Chemical Physics. 1962;37(11):2631-2645.

[11] Szabo J, Robin M, Paintal S, Pote B, Hruby V, Freeman C. Iodine Propellant Space Propulsion. 33rd International Electric Propulsion Conference. 2013.

[12] Thomas Domonkos M. Evaluation of low-current orificed hollow cathodes [Ph.D]. The University of Michigan; 1999.

[13] Tsay M, Frongillo J, Model J, Zwahlen J, Barcroft C. Neutralization Demo and Thrust Stand Measurement for BIT-3 RF Ion Thruster. 53rd AIAA/SAE/ASEE Joint Propulsion Conference. 2017.